TFY4235 - The World of Quantum Mechanics

Karl Kristian Ladegård Lockert[a]

[a] *Institutt for fysikk, Norges Teknisk-Naturvitenskapelige Universitet, N-7491 Trondheim, Norway.*

Abstract

When implementing different methods for solving the Schrödinger equation, we investigate the results and possible errors for three different systems, starting with a particle in a box. The computed energy eigenvalues are in good agreement with the analytic results for lower energies. Introducing a potential barrier to the box, a tunneling phenomena occurs when preparing an initial state out of (almost) degenerate states and propagating over a suitable time span. Propagating the same initial state with the Crank-Nicolson scheme gives zero tunneling in the same time interval as in the plane-wave basis. The Euler-scheme is found unfit, attributed to the requirement of H being unitary, which is not fulfilled. A relationship between the number of steps we are able to calculate (in the Euler scheme) and the discretization size, both spatial and temporal, is established. Lastly, a two-level system is studied. A numerical implementation of the time-evolution is presented,and used to compute the transition probabilities between two states. This is a result in good agreement with analytic approximations, with the added decoherence lowering the probability amplitude over time.

1. Introduction

This assignment on "The World of Quantum Mechanics" is about different methods for computing properties of different quantum systems. We will investigate numerical solutions of different one-dimensional quantum mechanical systems, all described by the Schrödinger equation

$$i\hbar\frac{\partial\psi}{\partial t} = H\psi. \tag{1}$$

Starting with a particle in a box, we succsessfully express the full wave function as a linear combination of *instantaneous* eigenstates. These are solutions of the time-independent Schrödinger equation

$$H\psi_n = E_n\psi_n. \tag{2}$$

Introducing a potential barrier to the box, a tunneling phenomena occurs when preparing an initial state out of (almost) degenerate states, and propagating this state over a suitable time span. For numerical evolution in time, two schemes are implemented. Both Euler, and Crank-Nicolson are able to reproduce the results obtained in the expansion of eigenstates, but the Euler-scheme requires a far finer discretization than what is computationally feasible. For a third system, presented with a time-dependent Hamiltonian, we discretize the Volterra integral equation for the formal solution of Equation (1).

All of the implementations are written in Python 3.7, with heavy utilization of optimized libraries. These libraries include SciPy for linear algebra, NumPy for array manipulations and vectorization, dask for parallellization of multiple solvers at once, and Numba for "just-in-time"-compilation of functions.

The treatment of the problems will be done in reduces units. Throughout the report, quantities with a bar ($\bar{A}$) that may have an analytic counterpart (A), will represent quantities which are (to be) computed where it is not clear.

2. Quantum mechanics in a box

The Schrödinger equation tells us the time-evolution of the wave function, which, according to the Copenhagen interpretation of quantum mechanics, has the physical interpretation of a probability amplitude when squaring the absolute value. In our current setup, where we have

$$V = \begin{cases} 0, & 0 < x < L \\ \infty, & \text{otherwise} \end{cases}, \tag{3}$$

there is 0% chance of finding the particle inside the "walls" (at $x < 0$ or $x > L$). Thus, the wave function must go to zero at these points. Defining $x' = x/L$ and $t' = t/t_0$, and inserting in Equation (1).

$$\begin{aligned} i\hbar\frac{\partial\psi}{\partial t} = i\hbar\frac{\partial\psi}{\partial t'}\frac{\partial t'}{\partial t} &= \frac{-\hbar^2}{2mL^2}\frac{\partial^2\psi}{\partial x'^2} \\ \implies i\frac{\partial\psi}{\partial t'} &= \frac{-\hbar}{2mL^2\frac{\partial t'}{\partial t}}\frac{\partial\psi}{\partial x'^2} \end{aligned}$$

Thus, setting

$$t' = \frac{\hbar}{2mL^2}t, \quad x' = \frac{x}{L} \tag{4}$$

gives the wanted dimensionless equation

$$i\frac{\partial\psi}{\partial t'} = -\frac{\partial^2\psi}{\partial x'^2}. \tag{5}$$

Inserting our new variables in Equation (2) with

$$H = \frac{\hat{p}^2}{2m} + V(x) = -\frac{-\hbar}{2mL^2}\frac{\partial^2}{\partial x'^2} + \tilde{V}(x'),$$

we get

$$\begin{aligned} \frac{-\hbar^2}{2mL^2}\frac{\partial^2\psi_n}{\partial x'^2} = E_n\psi_n \implies \\ -\frac{\partial^2\psi_n}{\partial x'^2} = \lambda_n\psi_n, \end{aligned} \tag{6}$$

with the relation

$$\lambda_n = \frac{2mL^2E_n}{\hbar^2} \tag{7}$$

between the energy levels and the dimensionless eigenvalues. The boundary conditions that the wave function disappears in the walls, but the walls are now at $x' = 0$ and $x' = 1$. It is now clear that choosing $x_0 = L$ is suitable, as it makes us able to work on the simple domain $[0, 1]$. Any other proportionality constant $\alpha \in \mathbb{R}$ such that $x' = \alpha x/L$ should work as well, scaling both the time and energies by a factor α^2, as long as x' is dimensionless. Other scaling possibilities are also possible, and have consequences for the analytic expressions for ψ. For example scaling the interval to be mirrored about $x = 0$ would only pick out the even terms in a Fourier series expansion.

Solving Equation (6) with the imposed boundary conditions can be done analytically in the following manner. Since we are looking for solutions that have self-similar second derivatives with an extra minussign, we guess a solution on the form $\psi = A_n \sin\left(\sqrt{\lambda_n}x'\right) + B_n \cos\left(\sqrt{\lambda_n}x'\right)$. The boundary condition $\psi(x' = 0) = 0$ gives $B_n = 0$, while the boundary condition $\psi(x' = 1) = 0$ gives the restriction to λ_n that $\sqrt{\lambda_n} = n\pi$, hence the labels n are also justified. Our analytic solution is therefore

$$\psi_n(x') = \mathcal{N}\sin(\pi n x'), \tag{8}$$

where $\mathcal{N}$ is a normalization constant to be decided.

$$\begin{aligned} 1 = \langle\psi_n|\psi_n\rangle = \mathcal{N}^2\int_0^1 \mathrm{d}x' \sin^2(n\pi x') \\ = \mathcal{N}^2\int_0^1 \mathrm{d}x' \frac{1-\cos(2\pi n x')}{2} = \frac{\mathcal{N}^2}{2} \\ \implies \mathcal{N} = \sqrt{2}, \end{aligned}$$

and we have the analytic solution as announced in [1].

The implementation of a finite-difference-scheme is done using sparse matrix formatting for the cases when the discretization step is very small. Otherwise a dense matrix format is sufficient for solving eigenvalues, using the "eigsh"-function from NumPy's linear algebra library.

In Figure 1 a comparison of the calculated eigenvalues against both the analytic expression for λ_n and n is shown for the case where the interval is discretized in 5000 points.

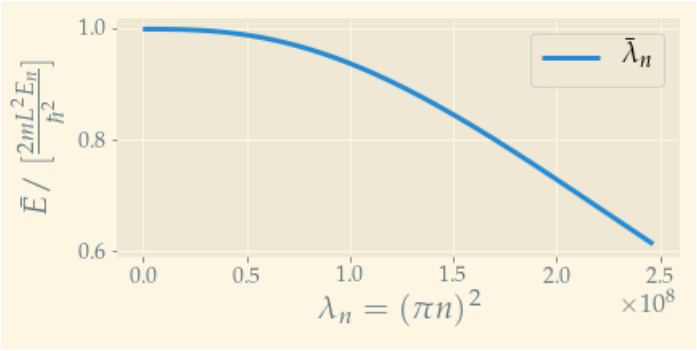

(a) Computed eigenvalues against the analytic expression.

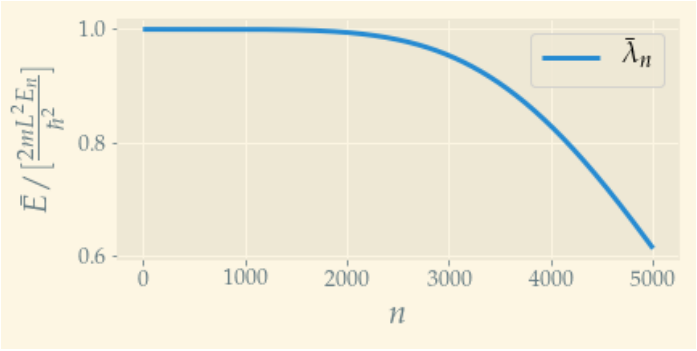

(b) Computed eigenvalues against n.

Figure 1: Comparison of computed eigenvalues and the analytic expressions.

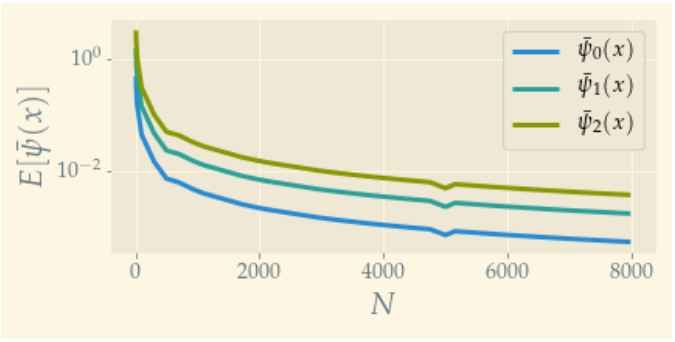

Figure 2: Error of the ground state, first- and second excited states as a function of the discretization steps.

Notice that $\bar{\lambda}_n/\lambda_n$ is close to 1 for n up to about 2000, where the energies are 2000^2 times higher than the ground state.

To compute the error of a numerical solution, we must have a metric of some sort. Let us introduce

$$E[\bar{\psi}_n(x')] = \int \mathrm{d}x' \, ||\bar{\psi}_n(x')| - |\psi_n(x')||^2 \tag{9}$$

as an example, where the bar denotes the numerical approximation to the analytic function. Then, a comparison of the eigenvectors with respect to the number of discretization steps can be made. In Section 2, this is shown

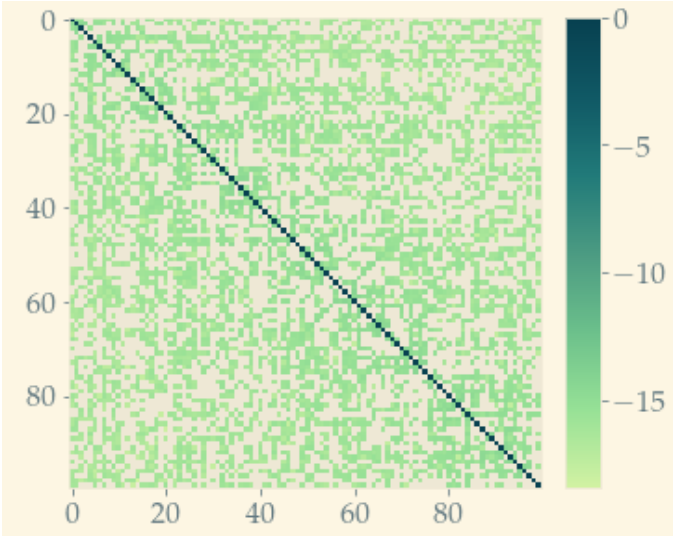

Figure 3: Logarithm (base 10) of the inner product of the 100 lowest excited eigenfunctions.

for the three lowest energy levels.

The implementation of

$$\alpha_n = \langle \psi_n | \Psi_0 \rangle = \int \mathrm{d}x' \, \psi_n^*(x') \Psi_0(x') \tag{10}$$

can be done in a simple fashion by taking optimized inner-product implementations for general vectors, so calculating the actual integral is actually not needed. In Figure 3, the inner product of the first 100 eigenfunctions are shown, and indicates orthogonality of the states. The off-diagonals are ~ 15 orders of magnitude smaller than the diagonal, which we might attribute to numerical artifacts or the imperfectness of the solutions, which we have seen is present, c.f. Figure 1 and Section 2.

Using the reduced units previously discussed, we can express the full state

$$\Psi(x,t) = \sum_n \alpha_n \exp\left(-\frac{iE_n t}{\hbar}\right)\psi_n(x) \tag{11}$$

as

$$\begin{aligned}\sum_n \alpha_n \exp\left(-\frac{iE_n t}{\hbar}\right)\psi_n(x) &= \sum_n \alpha_n \exp\left(-\frac{iE_n t}{\hbar}\right)\psi_n(x) \\ &= \sum_n \exp\left(-\frac{i\frac{\hbar^2\lambda_n}{2mL^2}\frac{2mL^2 t'}{\hbar}}{\hbar}\right)\psi_n(x') \\ \implies \Psi(x',t') &= \sum_n \alpha_n \exp(-i\lambda_n t')\psi_n(x'). \end{aligned} \tag{12}$$

Now using the ground state

$$\Psi_0 = \sqrt{2}\sin(\pi x) \tag{13}$$

as initial condition, we can compute the full state. In Figure 4 the initial states are plotted both for the analytic expression and the computed value at $t = 0$. The normalization is also well-defined, as seen in Figure 5. For Ψ_0 as in Equation (13), this is expected, since Ψ_0 is orthogonal to $\Psi_{i\neq 0}$, and Ψ_0 is properly normalized itself. For $\Psi_0 = \delta(x' - 1/2)$, however, this is more complicated. In this case, $c_n = \int \mathrm{d}x' \, \psi_n^* \delta(x' - 1/2)$ gives $c_n = \psi_n$, which means that only half of the eigenfunctions in Equation (8) will contribute. Numerically, however, we can only estimate the value of the Dirac-delta with a finite number of plane waves, in contrast to its integral representation $\delta \sim \int \mathrm{d}k \, \mathrm{e}^{ikx}$.

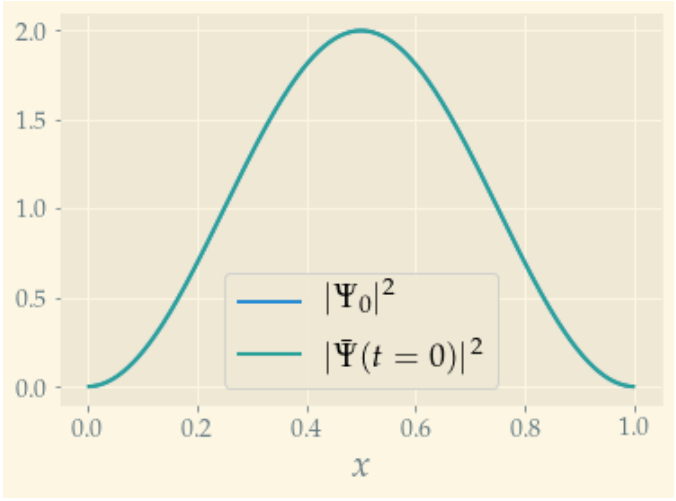

Figure 4: Analytic and computed probability density of initial state Ψ_0 using $N = 1000$ as the number of discretization points

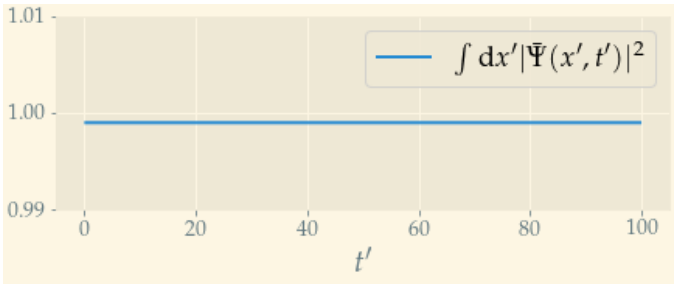

Figure 5: Normalization of the computed wave function for the time interval $t' \in [0, 100]$ width $N = 10000$ and $\Psi_0(x') = \delta(x' - \frac{1}{2})$.

3. Adding a barrier to the box-potential

Let us now consider a potential barrier in the box, modeled by the dimensionless potential $\nu(x') = t_0 V_0/\hbar$, where $t_0 = \frac{2mL^2}{\hbar}$ as in Equation (4), and is given by

$$\nu(x') = \begin{cases} 0, & 0 < x' < \frac{1}{3} \\ \nu_0 = \frac{2mL^2 V_0}{\hbar^2}, & \frac{1}{3} < x' < \frac{2}{3} \\ 0, & \frac{2}{3} < x' < 1 \\ \infty, & \text{otherwise} \end{cases} \tag{14}$$

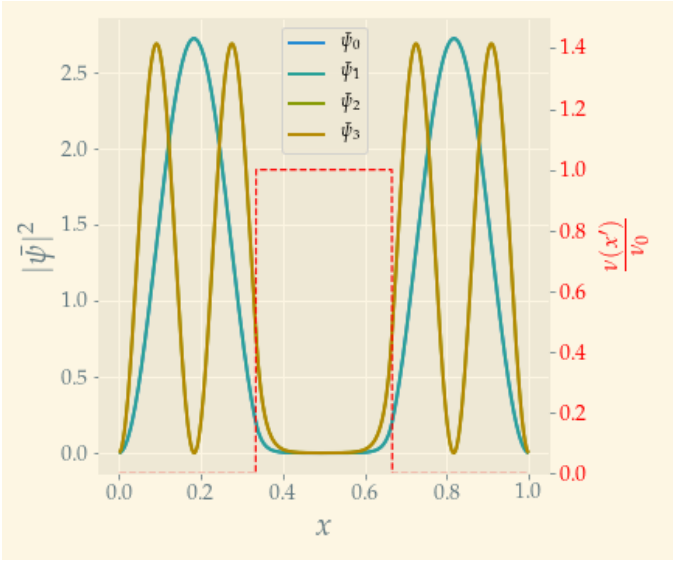

Figure 6: Degeneracy of the ground state and first excited states plotted together with the potential.

Thus, setting ν_0 to 0 is the same task as we had for the previous case, since we have the same boundary conditions and a vanishing potential between the edges, which ensures that the matrix-representation (and thus the eigenvalues) of the operator acting on the wave function is equal. Now we set $\nu_0 = 10^3$. Comparing the energy eigenvalues for the problem, we find that some seem to be equal, i.e. there seems to be degeneracy in the system. This cannot be, since we are in 1D with a discrete energy spectrum [2]. Indeed, the states are equal, as we can see for the lowest lying energy eigenfunctions in Figure 6. We now prepare the initial state

$$\Psi_0 = \frac{1}{\sqrt{2}} \left(\psi_1(x') + \psi_2(x') \right) \tag{15}$$

and let it evolve from $t'_0 = 0$ to

$$t'_1 = \frac{\pi}{\lambda_2 - \lambda_1}, \tag{16}$$

we find that the particle has tunneled from one side of the barrier to the other! This is shown in Figure 7. We can see that the initial state (on the left side of the potential barrier) "leaks" into the opposite side as time progress. Inserting Equation (16) into Equation (12), we find (after some manipulation)

$$\Psi(x', t'_1) = C \left(\psi_2(x') - \psi_1(x') \right) \tag{17}$$

for a normalization constant C. This is the initial state mirrored about $x' = 1/2$.

3.1. Root finding

Following ref. [1], the eigenvalues of the analytic solutions are given by the roots of the function $f(\lambda)$, shown in Figure 8. This is in good agreement with the computed

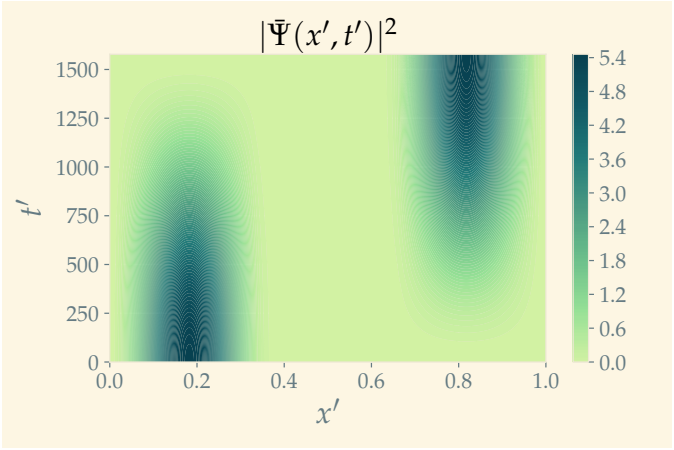

Figure 7: Tunneling across the potential barrier.

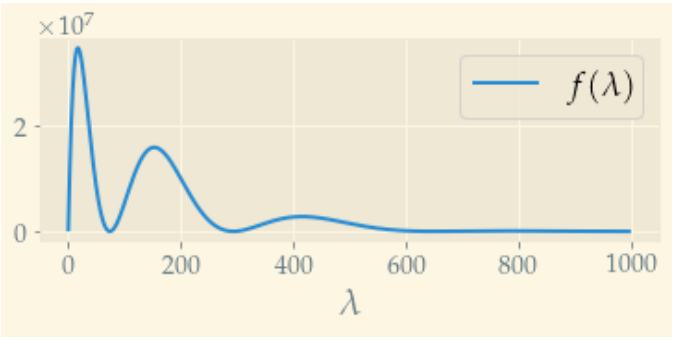

Figure 8: The analytic expression for finding the eigenvalues.

eigenvalues. By using SciPy's [3] optimized root-finding algorithm with the computed eigenvalues as the initial guess, we find three distinct eigenvalues below $\nu_0 = 10^3$. Using the implementation of the root finder, the roots of $f(\lambda)$ is found more precicely, and the first couple of roots are shown in Table 1. Investigating the roots of $f(\lambda)$ for different values of ν_0, we find that the value of ν_0 that separates having one and no states with $\lambda < \nu_0$ is for

$$\nu_0 = 22.10526(3). \tag{18}$$

Computed λ	Roots of $f(\lambda)$
73.49662578	73.93560016
73.49861656	
291.77230762	293.49231502
291.79660664	
644.62162712	648.26437316
645.10279446	

Table 1: A comparison of computed eigenvalues and computed roots of the analytic expression for $f(\lambda)$. The units are given by Equation (7).

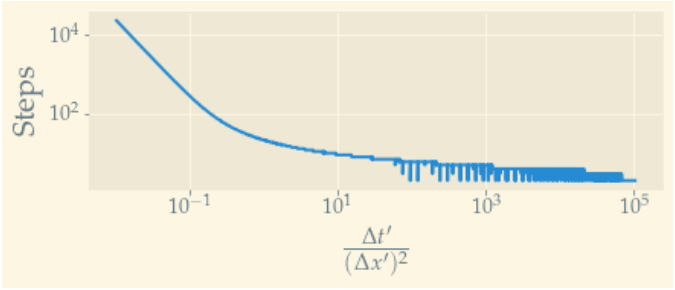

Figure 9: The number of steps taken before the Wave Function breaks down against the Courant-Friedrichs-Lewy (CFL)-number on a log-log scale.

4. Step-by-step time evolution

For a time-dependent Hamiltonian, an expansion in stationary eigenstates does not work in the same simple fashion. This is because the states ψ_i are eigenvectors of the *instantaneous* Hamiltonian. For different times , these vectors are not any more eigenvectors of the full Hamiltonian. That being said, with a step-by-step implementation we should get rid of the apparent degeneracy of the eigenvalues.

4.1. Euler scheme

We now implement the Euler scheme for evaluating its applicability for the quantum problem. An interesting phenomena occur, where the function abruptly breaks down after a number of time steps. The approach to finding the number of steps before this breakdown is by looking at the normalization of the wave function. As this suddenly diverges, we can use this as a check in a while-loop for comparing step sizes in both temporal and spatial direction.

In Figure 9 the steps before the breakdown of the simulation for the Euler-Scheme is shown. This suggests that for the a successful simulation in this scheme, we need $\Delta t' \ll (\Delta x')^2$. At thee same time we also want $\Delta x' \ll 1$, so this would require a very heavy computation. A better approach is to use a different numerical scheme.

4.2. Crank-Nicolson

The implementation of this scheme is done by computing the LU-decomposition of $\left(1 + \frac{i}{2}\Delta t' \hat{H}\right)$ and solving a linear system $A\mathbf{x} = b$ for each time step. As previously mentioned, we should get rid of the degeneracy of states. With this in mind, the phase $\sim \frac{1}{\lambda_2 - \lambda_1}$ should diverge, and we have to propagate the system infinitely in time. By preparing the same state as in Equation (15), we can use the Crank-Nicolson scheme to propagate the function and check this. As viewed in Figure 10, there is now no tunneling, as opposed to the case when we project the states on a plane-wave basis, c.f. Figure 7.

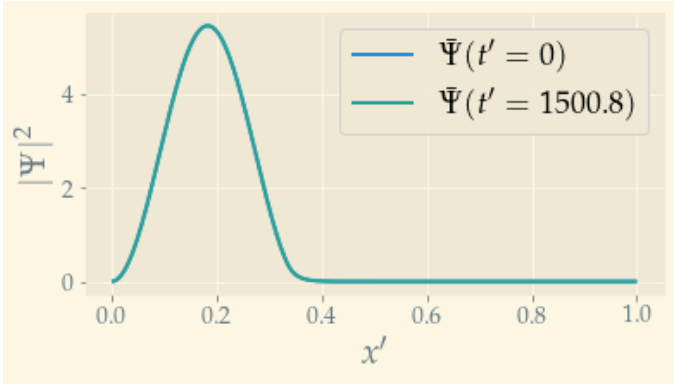

Figure 10: Initial state and time-evolved state using the Crank-Nicolson scheme.

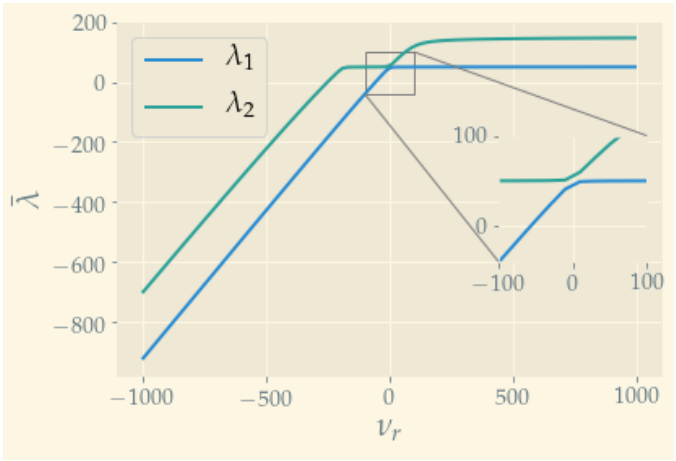

Figure 11: The two lowest eigenvalues plotted against the varying potential ν_r.

4.3. Two level system

Figure 11 shows the two lowest lying energy eigenvalues for $V(x,t)$ as introduced in ref.[1]. For $\nu_r = 0$, the energy difference is $\varepsilon_0 \simeq 5.6962$.

The expectation value

$$\tau = \langle g_0 | \hat{H} | e_0 \rangle \tag{19}$$

can be computed as the previous inner products, applying first the action of $\hat{H}$ to $|e_0\rangle$ and then taking the inner product. τ is found to take a linear shape

$$\tau(\nu_r) \simeq -0.429\nu_r. \tag{20}$$

Let us next discretize the Volterra integral equation

$$|\psi(t = k\Delta t)\rangle_I = |\psi(0)\rangle - \frac{i}{\hbar}\int_0^t \mathrm{d}t'\, H_{1I}(t')\,|\psi(t')\rangle_I \tag{21}$$

using the Trapezoidal rule

$$\int_0^t f(t)\,\mathrm{d}t \simeq \sum_{k=1}^{N} \frac{f((k-1)\Delta t) + f(k\Delta t)}{2}\Delta t. \tag{22}$$

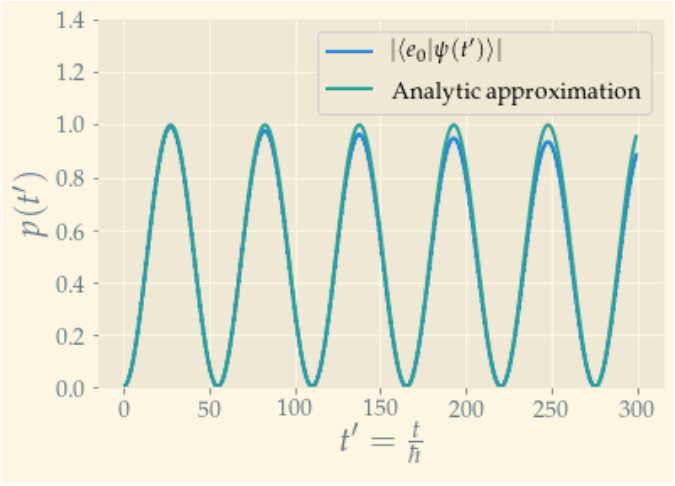

Figure 12: The probability of finding the system in the first excited state, $|e_0\rangle$.

We get

$$
\begin{aligned}
|0\rangle &= |0\rangle \\
|\Delta t\rangle &= |0\rangle - \frac{i}{\hbar}\Delta t H(0)\,|0\rangle \\
|2\Delta t\rangle &= |0\rangle - \frac{i}{\hbar}\Delta t\,(H(0)\,|0\rangle + H(\Delta t)\,|\Delta t\rangle) \\
&\vdots \\
|n\Delta t\rangle &= |0\rangle - \frac{i}{\hbar}\Delta t\left(\sum_{k=1}^{n-2} H(k\Delta t)\right. \\
&\qquad \left. + \frac{H(0)\,|0\rangle + H((n-1)\Delta t)\,|(n-1)\Delta t\rangle}{2}\right).
\end{aligned}
$$

The implementation of this discretization could be done by clever matrix manipulations. It could also be done with a simpler implementation, looping over all states previously calculated. This is a more "brute-force" way of doing it, but works. In Figure 12 a comparison of the implementation and an approximate solution for the probability of finding $|e_0\rangle$ given that the system was initially in $|\Psi(t=0)\rangle = |g_0\rangle$. This was done for $\omega = \varepsilon_0$ and $\tau = 0.02\varepsilon_0$. Notice the decoherence that occur in the computed probability, not present in the analytic expression[1]

$$p(t) = \sin^2\left(\frac{t\tau}{2\hbar}\right). \tag{23}$$

If we now vary ω and τ, we may notice the following. Setting $\omega \neq \varepsilon_0$ will lower the probability of finding the system in the state $|e_0\rangle$, and shifting the peaks. Increasing τ does not seem to alter the amplitude of the probability, but shifts the peaks to earlier times. This is visualized in Figure 13, where secondary oscillations are more pronounced than in Figure 12. If we choose τ too large, the method breaks down. This is clear from an interpretation of τ as a perturbation smallness parameter, in which a perturbation series would diverge for $\tau > 1$.

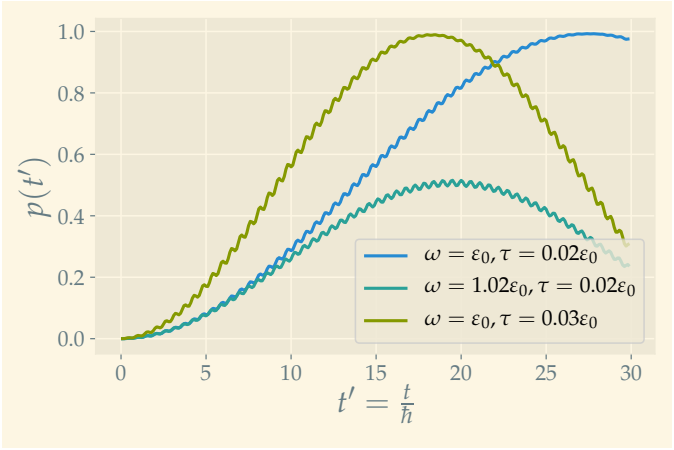

Figure 13: The transition probability $|\langle g_0|\psi(t)\rangle|^2$ of three different configurations.

References

[1] J. T. Kjellstadli, A. Sala, and I. Simonsen. Assignment 3: The world of quantum mechanics. `http://web.phys.ntnu.no/~ingves/Teaching/TFY4235/Assignments/TFY4235_Assignment_03.pdf`, 2020.

[2] Per Christian Hemmer. *Kvantemekanikk*. Tapir Akademiske Forlag, 5 edition, 2005.

[3] Pauli Virtanen, Ralf Gommers, Travis E. Oliphant, Matt Haberland, Tyler Reddy, David Cournapeau, Evgeni Burovski, Pearu Peterson, Warren Weckesser, Jonathan Bright, Stéfan J. van der Walt, Matthew Brett, Joshua Wilson, K. Jarrod Millman, Nikolay Mayorov, Andrew R. J. Nelson, Eric Jones, Robert Kern, Eric Larson, CJ Carey, İlhan Polat, Yu Feng, Eric W. Moore, Jake Vand erPlas, Denis Laxalde, Josef Perktold, Robert Cimrman, Ian Henriksen, E. A. Quintero, Charles R Harris, Anne M. Archibald, Antônio H. Ribeiro, Fabian Pedregosa, Paul van Mulbregt, and SciPy 1. 0 Contributors. SciPy 1.0: Fundamental Algorithms for Scientific Computing in Python. *Nature Methods*, 17:261–272, 2020.